© 2015. Published by The Company of Biologists Ltd | Journal of Experimental Biology (2015) 218, 3941-3949 doi:10.1242/jeb.127340

RESEARCH ARTICLE

Morphology does not predict performance: jaw curvature and prey crushing in durophagous stingrays

Matthew A. Kolmann[1,*], Stephanie B. Crofts[2], Mason N. Dean[3], Adam P. Summers[4] and Nathan R. Lovejoy[5]

ABSTRACT

All stingrays in the family Myliobatidae are durophagous, consuming bivalves and gastropods, as well as decapod crustaceans. Durophagous rays have rigid jaws, flat teeth that interlock to form pavement-like tooth plates, and large muscles that generate bite forces capable of fracturing stiff biological composites (e.g. mollusk shell). The relative proportion of different prey types in the diet of durophagous rays varies between genera, with some stingray species specializing on particular mollusk taxa, while others are generalists. The tooth plate module provides a curved occlusal surface on which prey is crushed, and this curvature differs significantly among myliobatids. We measured the effect of jaw curvature on prey-crushing success in durophagous stingrays. We milled aluminum replica jaws rendered from computed tomography scans, and crushed live mollusks, three-dimensionally printed gastropod shells, and ceramic tubes with these fabricated jaws. Our analysis of prey items indicate that gastropods were consistently more difficult to crush than bivalves (i.e. were stiffer), but that mussels require the greatest work-to-fracture. We found that replica shells can provide an important proxy for investigations of failure mechanics. We also found little difference in crushing performance between jaw shapes, suggesting that disparate jaws are equally suited for processing different types of shelled prey. Thus, durophagous stingrays exhibit a many-to-one mapping of jaw morphology to mollusk crushing performance.

KEY WORDS: Myliobatidae, Biomaterials, Rapid prototyping, Toughness, Bite force

INTRODUCTION

Batoids (rays, skates, sawfishes and guitarfishes) comprise over half of the cartilaginous fish diversity and include several lineages that independently evolved hard prey crushing. The myliobatid stingrays are a monophyletic group in which the members either eat shelled prey that exhibit high toughness, stiffness, and/or strength (Myliobatinae, Rhinopterinae, Aetobatinae), or have abandoned biting altogether and filter feed (Mobulinae) (Summers, 2000; Aschliman, 2014). Myliobatid stingrays arose approximately 65–70 mya, coincident with the rise of other durophagous fishes as well as a shift in the ecomorphological structure of molluscan communities (Vermeij, 1977; Aschliman et al., 2012). Compared with non-durophagous stingrays, myliobatids have reduced cranial mobility (e.g. caused by jaw symphyseal fusion), several instances of duplicated or reoriented muscles, and increased skeletal reinforcement, all features convergent with other durophagous vertebrates (Summers, 2000; Kolmann et al., 2014; Mulvany and Motta, 2014). Durophagous stingrays also feature robust teeth, interlocking at their bases to form shallow-domed tooth plate arrays (Fig. 1). Batoids and sharks have continuous dental replacement; in durophagous ray tooth modules, younger teeth mineralize and are conveyed labially to replace older, worn teeth.

Myliobatid rays have considerable inter-taxon variation in the morphology of the jaw complex, with the jaws and teeth varying in overall shape, length, width, and cross-sectional curvature (Fig. 1). Some species, such as eagle rays (*Aetobatus narinari*), prey almost exclusively on gastropods (Schluessel et al., 2010), while others, such as bat rays (*Myliobatis*), appear to prey preferentially on decapods (Gray et al., 1997; Szczepanski and Bengston, 2014) (Fig. 1). Finally, cownose rays (*Rhinoptera*) feed on a wide variety of hard and soft prey, depending on geographic distribution (Collins et al., 2007; Ajemian and Powers, 2012). By examining how performance differs among jaw shapes, we may be able to determine whether disparate jaw shapes are optimized for crushing different types of hard prey.

The crushing of hard prey provides a simple, direct, and useful performance metric for investigating the relationship between form and function. There is little ambiguity in deciding whether a prey item has been crushed, so there is a clear relationship between morphology and performance. The main determinant of predator success is the ability to exert high loads (Pfaller et al., 2011). For this reason it is possible to explore the implications of different predator and prey morphologies and to determine their interactions (Bertness and Cunningham, 1981; Whitenack and Herbert, 2015). Not only is there variation in the crushing jaws of the predators, but there are also material and structural differences in the shells of the prey. Mollusk taxa differ in the microstructure of the material that comprises the shell (involving so-called fibrous, prismatic, cross-lamellar, or nacreous mineral-organic composite layers or combinations of these), and the incorporated polymorphs of calcium carbonate mineral (aragonite and/or calcite). The relationship between taxon-specific structural differences and shell mechanics is yet to be clarified, but it is clear that the organic component of the composite layers results in drastic increases in shell toughness, relative to aragonite or calcite alone (Currey, 1980).

The simple metric of crushing allows us to ask whether the predator's morphology is a strong predictor of feeding performance or whether crushing success is more contingent on morphological (structural) and/or material composition of the shells of prey. Here, we investigate the effect that variation of jaw shape in durophagous stingray taxa has on crushing success. Our study had four goals: (1) compare jaw cross-sectional curvature among four species of

[1]Department of Ecology and Evolutionary Biology, University of Toronto at Scarborough, 1265 Military Trail, Toronto, Ontario, Canada M1C 1A4. [2]Department of Biological Sciences, New Jersey Institute of Technology, University Heights, Newark, NJ 07102, USA. [3]Department of Biomaterials, Max Planck Institute of Colloids and Interfaces, Am Muehlenberg 1, 14424 Potsdam, Germany. [4]Friday Harbor Laboratories, University of Washington, 620 University Dr., Friday Harbor, WA 98250, USA. [5]Department of Biological Science, University of Toronto at Scarborough, 1265 Military Trail, Toronto, Ontario, Canada M1C 1A4.

*Author for correspondence (matthew.kolmann@mail.utoronto.ca)

Received 29 June 2015; Accepted 21 October 2015

Journal of Experimental Biology (2015) 218, 3941-3949 doi:10.1242/jeb.127340

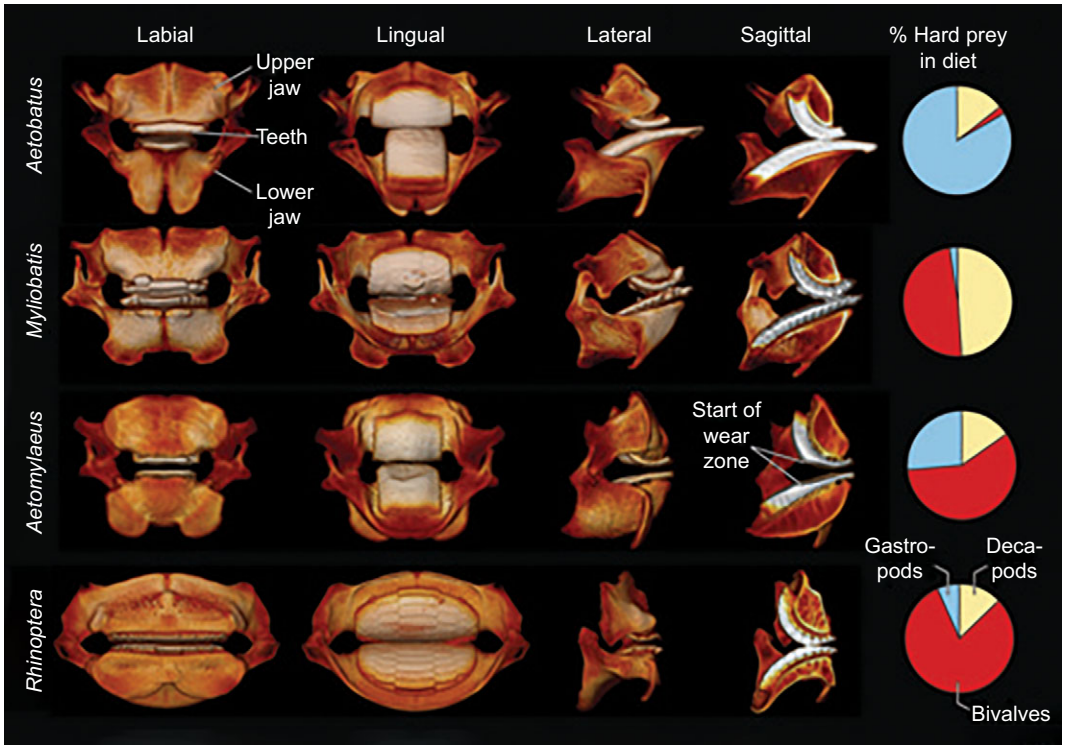

Fig. 1. External and internal jaw morphology of myliobatid rays. Computed tomography (CT) scans of *Aetobatus narinari*, *Myliobatis californica*, *Aetomylaeus bovinus*, and *Rhinoptera bonasus* (top to bottom) in labial, lingual, lateral, and sagittal views (left to right). Prey contribution to dietary proportions based on % frequency or % index of relative importance of decapods, bivalves, and gastropods. Diet data are from Schluessel et al. (2010), Gray et al. (1997), Capape (1977), and Ajemian and Powers (2012) (in the same order as species).

durophagous stingrays, and evaluate metrics for this comparison; (2) use physical models (jaw replicas) from the four durophagous stingrays to compare crushing performance; (3) quantify and compare differences in performance for the crushing of live prey items, complex physical models, and simple physical models; and (4) quantify the 'crushability' of three different species of mollusk (one gastropod and two bivalves).

Shelled prey are not all created equal in terms of the mechanical properties of their shells; we investigated three parameters of crushing performance (peak load, yield load, and work-to-fracture/toughness; Fig. 2), the combination of which characterizes the ability of shelled prey to absorb energy before fracture (toughness) and to withstand forces (stiffness) before total failure, illuminating mechanical differences in prey exoskeletons and jaw performance. Yield loading, designated here as the amount of force required to plastically deform the shell (indent) is contrasted with peak loading, the amount of force required to fail the shell outright (Fig. 2).

MATERIALS AND METHODS

Jaw replica construction and jaw metrics

Whole specimens of *Aetomylaeus nichofii* (Bloch & Schneider, 1801), *Aetobatus narinari* (Euphrasén, 1790), *Myliobatis tobijei* (Bleeker, 1854), and *Rhinoptera bonasus* (Mitchill, 1815) were obtained from museum collections during a prior study (Dean et al., 2007). These species represent the four extant genera of durophagous myliobatid rays, which cover the range of ecological variability in this clade. These specimens were computed tomography (CT) scanned with a 16-slice medical grade Siemens RS SOMATOM Sensation (MDCT-16, Siemens Medical Solutions, Malvern, PA, USA) with 0.75 mm slice thickness and helical-spiral scans. Specimen information can be found in the appendix of Dean et al. (2007). Specimens were wrapped in alcohol-saturated cheesecloth and scanned in large Ziploc© bags. Scans were reconstructed as 8 bit .TIFF stacks and rendered as three-dimensional (3D) visualizations using Amira software (v. 5.2.2, Visage Imaging, Inc., Richmond, VIC, Australia).

The upper and lower jaws (palatoquadrate and Meckel's cartilage, respectively) and tooth plates were segmented (digitally dissected) from the rest of the body. A medial sagittal section of each jaw complex (including jaws and teeth) was manually traced in Adobe Illustrator CS (Adobe

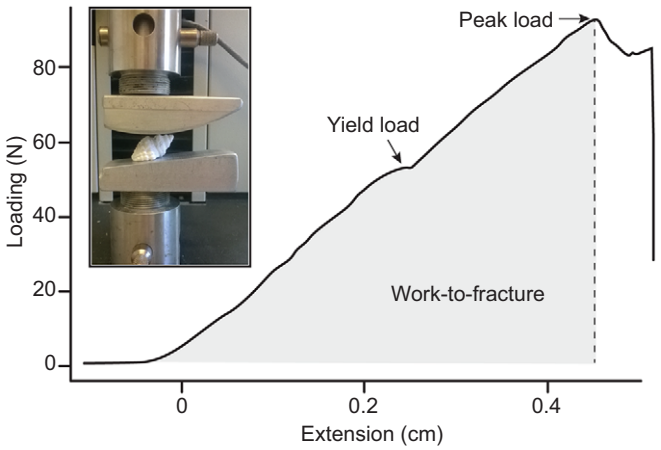

Fig. 2. Example force-displacement trace during crushing of live shells. Peak load (N) represents the maximum load (N) reached at shell fracture. Yield load (N) is represented by the characteristic slope change, suggesting plastic deformation of shell material prior to actual fracture. Work-to-fracture (Nm) was calculated as the area beneath the curve leading to peak loading. Inset shows mounted jaw replicas on a mechanical loading frame with a replica shell placed between the occlusal surfaces.

Journal of Experimental Biology (2015) 218, 3941-3949 doi:10.1242/jeb.127340

Systems, Inc., San Jose, CA, USA). These two-dimensional images were then extruded (extended into the *z*-axis), resulting in four pairs of simplified 3D jaw models scaled to 40 mm standard width and cropped to include only the relevant occlusal surface (in an anterior–posterior direction) in 123D Design (v. 1.4.51, Autodesk, Inc., San Rafael, CA, USA). This functional occlusal surface was determined by examining the pattern of wear on specimen tooth plates (e.g. note the wear in the lingual and sagittal images in Fig. 1). Jaw models were exported as .stl files into SprutCAM7 Pro (v. 7.1.5, Sprut Technologies, Inc., Tormach Inc., Waunakee, WI, USA) to generate tool paths for computer numerical controlled milling. Models were fashioned from 6061T aluminum stock using a four-axis mill (Tormach PCNC1100, Tormach Inc.), deburred with a belt sander, and polished (Fig. 2 inset image).

Radius of curvature of the occlusal surface of each jaw complex was measured by fitting a circle to the upper and lower jaw of each species using ImageJ. Larger curvatures correspond to increasingly 'flatter' or more broadly curved jaw sets, while smaller curvatures indicate a more peaked or domed morphology. We used two metrics to characterize the jaws of each species: (1) the average curvature of the upper and lower jaws together, and (2) a measure of the disparity between upper and lower jaw curvatures, which we generated by dividing the upper jaw curvature by the lower jaw curvature.

Prey

Several types of 'prey' were subjected to materials testing: (1) live common blue mussels (*Mytilus edulis* Linnaeus, 1758; shell height size range=6.0–20.5 cm), (2) live varnish clams [*Nuttalia obscurata* (Reeve, 1857); shell height size range=6.0–19.3 cm], (3) live frilled dogwinkles [*Nucella lamellosa* (Gmelin, 1791); shell height size range=6.0–23.3 cm], (4) 3D-printed replica shells (ZPrinter 310, ZCorporation, Inc,. Rock Hill, SC, USA) of the frilled dogwinkle *Nucella lamellosa* (1.0–2.5 cm, four size classes at 0.5 cm intervals), and (5) ceramic tubes (FluVal BioMax filter media rings, Hagen, Inc., Montreal, QC, Canada; size ranges: height=0.9–1.3 cm, length=1.3–2.1 cm, inner diameter=0.3–0.45 cm, outer diameter=0.9–1.3 cm). Replica shells were based on .stl files generated from micro-CT scans from Crofts and Summers (2014). Replica shells were printed in plaster, hardened using a solution of magnesium chloride and water, and then placed in a vacuum heater for 12 h to dry and harden. Ceramic tube dimensions were measured using ImageJ (v. 1.40, National Institutes of Health, Bethesda, MD, USA) prior to crushing. Live prey were measured with digital calipers. Replica shells and ceramic tubes represent our 'complex' and 'simple' artificial prey types, respectively.

Although the live prey species used in these experiments have not been reported from the diets of the rays in question, congeneric or confamilial taxa are known to be consumed by myliobatids (Capape, 1977; Gray et al., 1997; Yamaguchi et al., 2005; Jardas et al., 2004; Collins et al., 2007; Schluessel et al., 2010; Ajemian and Powers, 2012). Live shellfish size series were collected from the region around Friday Harbor, San Juan Island, WA, from the intertidal. Shell length, height, and depth were recorded for each specimen. Shell length (spire length) was measured from the tip of the spire to the tip of the siphon in dogwinkles and from the umbo to the anterior-most edge of the valves in mussels and clams. Shell width was measured from the maximum extent of lateral opercular gape in dogwinkles, and from the lateral-most extent of the valves in mussels and clams. Shell height was measured with the operculum lying flat to the vertical-most extent of the spire in dogwinkles, with height being the maximum distance from the upper and lower valves in mussels and clams. Shell height is presumed to be the shape parameter of greatest relevance to compression resistance, as it is orthogonal to the normal (compressive) loading scenario (Kolmann and Huber, 2009; Crofts and Summers, 2014).

Prey-crushing simulations

Aluminum jaw replicas were threaded and attached to a mechanical loading frame (Synergie 100, MTS Systems Corp.) coupled to a 500 N load cell (Fig. 2 inset image). To explore the ability of artificial prey types to mimic the failure of natural specimens, we measured the performance (peak load, yield load, and work-to-fracture) required by each set of jaws to crush ceramic media (n=20 per jaw), and live and printed *Nucella* shells (n=40 per jaw), all of approximately similar size. Shell spires were positioned facing lingually for gastropods (Fig. 2 inset image). Bivalves were placed with the hinge facing labially, as seen in videos of prey-handling events of some durophagous rays (Fisher et al., 2011). Shells were crushed using a compressive loading regime of 1.27 mm s^{-1} (Crofts and Summers, 2014). Peak load (N) and yield load (N) were determined from stress/strain curves generated by TestWorks4 software (v. 4.08, MTS Systems Corp.) and recorded after each trial. Work (Nm) was calculated using a custom R script that estimates the area under the load–displacement curve for each trial, with the maxima of the given loading event being the point at which peak load was achieved (Fig. 2).

Statistical analyses and experimental design

Wilks–Shapiro and Levene's tests were used to test for normality and equal variances as prerequisites for determining whether data should be transformed prior to further analyses. The interaction between shell size, jaw morphology, and prey type (tubes versus live or printed snails) were compared using ANCOVA, with prey type as a covariate. Because the size and shape of the prey items varied, especially in the live *Nucella* specimens, we also used an ordinary least-squares regression of prey height on crushing performance to determine the size-corrected residuals of loading or work-to-fracture, and tested these data against prey type using a two-way ANOVA. By contrasting the crushing performance across jaw morphologies between printed dogwinkles (n=40) and live *Nucella* (n=30) using ANCOVA with live versus printed as a covariate, we were also able to determine how material and structural properties of live shells contribute to differences in overall crushing performance.

To determine the effect of different shell sizes on jaw crushing performance, we used a two-way ANOVA to test four size classes (n=10 per jaw) of printed *Nucella* shells. Finally, we tested whether different jaw morphologies convey any inherent advantage to crushing live snail (n=30), mussel (n=15), and clam (n=15) shells, which vary considerably in shape and presumably material and structural properties. The interaction between jaw morphology and shell dimensions were investigated using two-way ANOVA. We also used an ordinary least-squares regression of prey height on crushing performance to determine the size-corrected residuals of loading or work-to-fracture, and tested these data against jaw morphology using ANOVA.

Post hoc Tukey's honest significant difference (HSD) tests were run on ANOVAs to determine pairwise differences between variables. All analyses

Table 1. Forces and work-to-fracture for artificial snails

Species	Jaw morphology	*r* curvature	Average curvature	Ratio curvature	Peak load (N)	Yield load (N)	Work (Nm)
Rhinoptera	More similar	**595.9**	547.7	0.84	90.0±38.4	55.8±28.9	29.9±20.3
		499.5			36.7–169.5	15.4–145.4	3.9–83.6
Aetomylaeus		**304.9**	580.2	2.81	90.3±47.3	55.7±36.2	27.8±23.0
		855.4			31.4–207.9	21.5–181.5	3.0–96.9
Myliobatis		**231.1**	535.5	3.63	100.9±42.4	64.3±34.1	27.5±19.2
		839.9			38.8–212.1	25.1–182.8	3.9–92.0
Aetobatus	More disparate	**152.4**	457.6	5.00	101.1±68.2	61.1±41.1	34.1±37.3
		762.8			22.6–350.8	15.2–180.2	4.6–173.7

Values are means±s.d.
Bold and *italic* values are the upper and lower jaw radius of curvature (*r* curvature), respectively.

Journal of Experimental Biology (2015) 218, 3941-3949 doi:10.1242/jeb.127340

Table 2. Forces and work-to-fracture for ceramic tubes

Species	Jaw morphology	*r* curvature	Average curvature	Ratio curvature	Peak load (N)	Yield load (N)	Work (Nm)
Rhinoptera	More similar	**595.9**	547.7	0.84	183.8±29.0	165.1±31.7	23.6±5.4
		499.5			131.1–235.2	108.5–229.2	15.5–33.5
Aetomylaeus		**304.9**	580.2	2.81	170.8±30.1	137.5±29.9	25.5±7.9
		855.4			121.0–254.4	88.0–224.5	16.9–53.3
Myliobatis		**231.1**	535.5	3.63	183.8±40.6	165.5±37.9	23.1±7.2
		839.9			128.1–273.3	109.3–251.5	13.5–46.5
Aetobatus	More disparate	**152.4**	457.6	5.00	173.4±39.7	145.2±36.1	21.9±7.1
		762.8			131.6–314.1	110.0–274.3	12.8–46.5

Values are means±s.d.
Bold and *italic* values are the upper and lower jaw radius of curvature (*r* curvature), respectively.

were run in R (v. 2.15.0, www.theRproject.org). Because such a diversity of statistical comparisons was made, illustrating these in figures or marking them in tables would be visually complicated. Instead, test results and statistical significance are listed in the text.

RESULTS

Data were found to be non-normally distributed and in some cases to show unequal variances among variables, and were subsequently transformed before further analyses (Table S1). Performance variables generally increased with shell height. The residuals of the regression of shell height on each performance variable were used as our size-corrected dataset (Table S2).

Differences in performance and morphology among stingray genera

Myliobatis had the broadest (flattest) occlusal surfaces when averaging both upper and lower jaws, followed by *Rhinoptera* and *Aetomylaeus*, whereas *Aetobatus* had the most curved jaw overall. *Rhinoptera* jaws showed the least amount of disparity in curvature between the upper and lower and jaws, and *Aetobatus* had the largest disparity in curvature (Tables 1–5).

Comparing between the myliobatid taxa, *Aetobatus* generally displayed lower performance values (i.e. lower peak and yield loads and work-to-fracture) when compared with *Aetomylaeus*, *Rhinoptera*, and *Myliobatis*, which exhibited similar peak and yield loads in addition to work-to-fracture. There were differences between taxa for peak load (F=3.211, P=0.0233), but not yield load (F=2.04, P=0.108), for all prey items. Tukey's HSD results showed differences in peak loading performance between *Aetobatus* and most other taxa (*Myliobatis*, P=0.036 and *Rhinoptera*, P=0.069). According to Tukey's HSD comparisons, yield loads were different for all prey types (P<0.0001). Work-to-fracture did not differ between stingray taxa (F=2.476, P=0.0615), and *post hoc* analyses show that work-to-fracture differed between *Aetobatus* and *Rhinoptera* only (P=0.048). However, mussels tended to have higher work-to-fracture than gastropods.

Overall, *Aetomylaeus*, *Rhinoptera*, and *Myliobatis* exhibited similar peak and yield loads and work-to-fracture, whereas *Aetobatus* had the lowest values for all performance metrics. There was an effect of predator jaw shape on peak loading across the three live prey categories (F=3.091, P=0.0279), and of prey type on yield load (F=177.46, P<2.0×10^{-16}).

Artificial versus natural prey types

Performance metrics (peak load, yield load, and work-to-fracture) varied by live prey type (Tables 1–3). Yield loads were different for all prey types (P<0.0001), and *post hoc* analyses showed differences between all pairwise comparisons of prey types (P=0.014) and between live and printed snail shells, which behaved more similarly to each other than either did to ceramic tubes (Fig. 3). Overall, when size was taken into account, ceramic tubes required greater loading forces (peak load and yield load) to initiate fracture than either live or replica *Nucella* snails (Fig. 3). Work-to-fracture did not differ among prey types (F=2.399, P=0.0925), and ceramic tubes were shown to have generally higher work-to-fracture values than live *Nucella* snails, albeit this was not significantly different (P=0.08).

Using a multiple regression framework to examine how much prey size affected crushing performance, prey type was found to be the most informative variable (35.3% of variance), followed by shell width (22.2%), shell height (21.5%), and shell length (19.2%) when explaining trends in peak loading. Yield load showed a similar trend, with prey type explaining over half (55.2%) of the model variance, followed by shell width (15.0%), shell height (14.4%), and shell length (14.5%). Finally, for work-to-fracture, prey type was again the most explanatory variable, explaining 33.5% of the variance, followed by shell width (22.6%), shell height (22.5%), and shell length (18%).

Crushing live prey

Live *Nucella* snails generally required 1.5 to 3.0 times greater force to crush or indent (peak and yield loading, respectively) than

Table 3. Forces and work-to-fracture for live snails (*Nucella* sp.)

Species	Jaw morphology	*r* curvature	Average curvature	Ratio curvature	Peak load (N)	Yield load (N)	Work (Nm)
Rhinoptera	More similar	**595.9**	547.7	0.84	276.9±104.4	200.4±85.4	57.9±28.8
		499.5			96.6–486.4	65.3–384.0	11.6–126.6
Aetomylaeus		**304.9**	580.2	2.81	281.8±121.4	206.0±102.9	60.9±44.2
		855.4			69.6–483.7	46.1–448.6	5.5–171.5
Myliobatis		**231.1**	535.5	3.63	276.4±133.9	207.0±118.8	61.2±36.9
		839.9			66.5–483.0	52.7–444.0	7.3–153.9
Aetobatus	More disparate	**152.4**	457.6	5.00	219.4±103.5	160.9±81.4	45.9±36.0
		762.8			53.4–436.3	37.4–336.1	4.1–165.3

Values are means±s.d.
Bold and *italic* values are the upper and lower jaw radius of curvature (*r* curvature), respectively.

Journal of Experimental Biology

Journal of Experimental Biology (2015) 218, 3941-3949 doi:10.1242/jeb.127340

Table 4. Forces and work-to-fracture for live mussels (*Mytilus* sp.)

Species	Jaw morphology	*r* curvature	Average curvature	Ratio curvature	Peak load (N)	Yield load (N)	Work (Nm)
Rhinoptera	More similar	**595.9**	547.7	0.84	147.6±65.58	60.16±33.39	54.61±32.8
		499.5			57.2–314.3	15.6–145.8	11.6–217.2
Aetomylaeus		**304.9**	580.2	2.81	159.5±60.85	58.16±33.48	84.65±41.9
		855.4			58.5–285.8	23.8–140.8	5.5–171.5
Myliobatis		**231.1**	535.5	3.63	151.1±69.11	57.62±22.07	69.36±43.1
		839.9			35.6–292.1	15.3–92.2	2.3–157.6
Aetobatus	More disparate	**152.4**	457.6	5.00	142.3±59.9	65.9±32.41	68.36±43.1
		762.8			56.4–237.5	20.3–121.2	2.9–165.3

Values are means±s.d.
Bold and *italic* values are the upper and lower jaw radius of curvature (*r* curvature), respectively.

varnish clams or mussels, and mussels failed under noticeably lower loads (1.8 to 3.2 times lesser) than the other prey items (Fig. 4, Tables 3–5). After correcting for size, differences between prey species were still significant for all performance metrics. *Nucella* required more force (peak load and yield load) to fail than the bivalves, but mussels required higher peak loadings to fracture than clams. When corrected for size, mussels required the greatest work-to-fracture (generally 1.25 times greater), followed by gastropods and then clams (Fig. 5).

There was also a notable effect of shell height on peak load (F=163.25, $P<2.0\times10^{-16}$) and yield load (F=234.97, $P<2.0\times10^{-16}$), with yield and peak loads increasing as shell height increased. Correcting for shell size, only prey type was significant for peak load (F=91.24, $P<2\times10^{-16}$), with *post hoc* comparisons showing that all prey taxa differed from one another ($P\leq1.01\times10^{-5}$). Similarly, after correcting for size, only prey type was predictive of yield load (F=155.9, $P<2.0\times10^{-16}$), with both bivalve taxa virtually indistinguishable from one another, but conspicuously different from *Nucella* ($P<0.0001$).

Both shell height and prey type were correlated with work-to-fracture (shell height, F=339.94, $P<2.0\times10^{-16}$; prey type, F=7.256, P=0.000878). However, as with the loading variables, once corrected for prey size, only prey type (F=42.28, $P=2.24\times10^{-16}$) was predictive of work-to-fracture, and *post hoc* comparisons showed that all prey taxa differed from one another ($P\leq7.0\times10^{-7}$) in terms of work-to-fracture.

When examining the effect of prey size on fracture mechanics explicitly, size consistently affected crushing performance across all trials, whereas predator species accounted for less than 2% of all variance. Not unsurprisingly, the larger the shell, the more difficult it was to crush in terms of both loading and work. Multiple regression results show that when all variables were included, shell size parameters, typically shell height, were the most explanatory variables for predicting fracture. For peak loads on natural prey, shell height and prey species were found to explain 33.7% and 31.5% of the variance, respectively. Yield load showed a similar trend, but with prey species explaining over half (55.6%) of the model variance, followed by shell height (25.4%) and shell length (11.0%). For work-to-fracture, only shell height (35.6%), shell length (26.9%), and prey type (20.6%) were informative.

Fracture behavior of prey items

Printed and live snails consistently showed crack formation at the base of the spire in almost all trials (Fig. 6). Crack propagation continued dorsally along the spire suture, paralleling the shell aperture. This pattern was repeated across shells regardless of shell size. Generally, live *Nucella* differed from both simple and complex prey models in having greater variability in the ranges of both loading and work required to fracture the shell, 2.2 to 3.0 times greater than those of artificial prey. Fracture in live clams and mussels typically started along the dorsal surface, beginning at the umbo and continuing along the right valve (dorsal, in this case) anteriorly. There was periodic failure at the conjoining margins of the valves as thinner material buckled outwards.

DISCUSSION

There are many differences in the feeding apparatus of durophagous rays, including the size, shape, insertion, and pennation of muscles, and the arrangement of connective tissue (Kolmann et al., 2014), but we cannot ascribe any performance difference to one of the most obvious differences in morphology – the shape of the jaws. With minor exceptions, the shape of myliobatid jaws had little effect on the crushing performance of hard prey, regardless of prey type. *Aetobatus* and *Rhinoptera*, at opposite ends of a curvature continuum (larger to smaller curvature ratio), had significant but small differences in the peak load required to crush some prey types. Rather than evidence for the superiority of *Rhinoptera*'s morphology, we take this to be indicative of the power of our test scheme, which revealed a difference of just 221 N (for *Rhinoptera*)

Table 5. Forces and work-to-fracture for live clams (*Nuttalia* sp.)

Species	Jaw morphology	*r* curvature	Average curvature	Ratio curvature	Peak load (N)	Yield load (N)	Work (Nm)
Rhinoptera	More similar	**595.9**	547.7	0.84	182.9±78.7	114.7±51.2	69.9±60.0
		499.5			72.0–373.2	53.1–253.1	13.5–217.2
Aetomylaeus		**304.9**	580.2	2.81	195.2±95.7	116.1±69.1	57.8±41.9
		855.4			50.8–335.9	26.1–257.5	7.7–112.4
Myliobatis		**231.1**	535.5	3.63	167.6±85.4	114.7±65.3	45.5±39.5
		839.9			32.3–288.5	18.9–229.5	2.3–157.6
Aetobatus	More disparate	**152.4**	457.6	5.00	166.7±84.8	105.9±65.9	53.3±40.9
		762.8			32.3–380.2	24.9–277.0	2.9–112.5

Values are means±s.d.
Bold and *italic* values are the upper and lower jaw radius of curvature (*r* curvature), respectively.

Journal of Experimental Biology (2015) 218, 3941-3949 doi:10.1242/jeb.127340

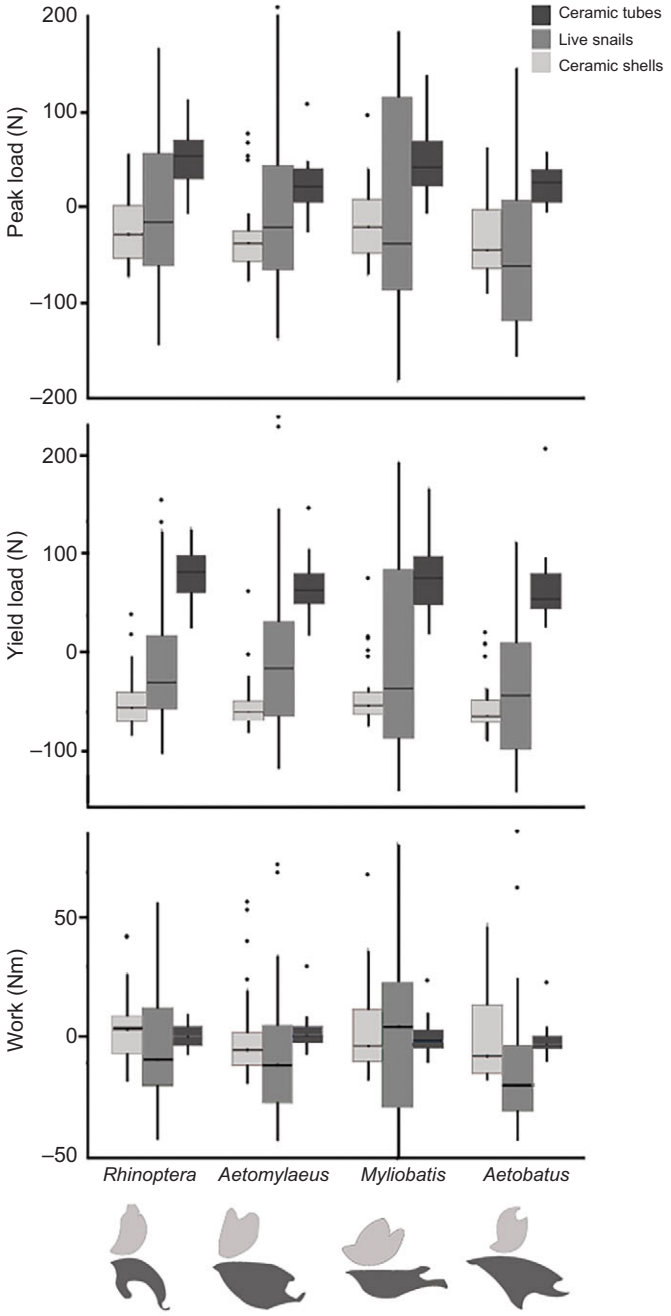

Fig. 3. Box whisker plots showing size-corrected crushing performance on artificial and natural prey. Ceramic filter tubes are in dark grey, live *Nucella* are in medium grey, and 3D-printed *Nucella* shells are in light grey. Performance is size-corrected by taking the residuals of the linear regression of shell height on the respective performance metric (peak and yield loading, work-to-fracture). Boxes represent 50% quantiles, bars represent median values, whiskers represent standard errors, and black dots represent outlying data. Jaw morphologies of each taxon are shown below.

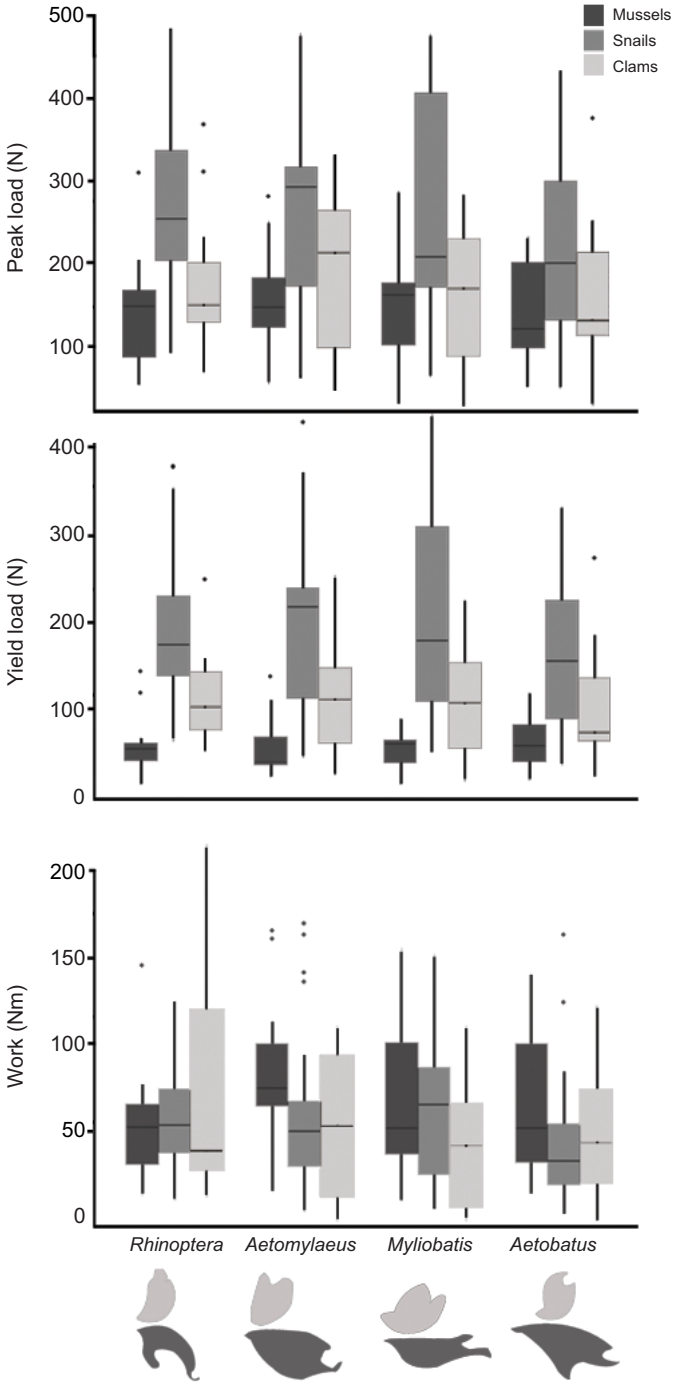

Fig. 4. Box whisker plots showing actual (not corrected for size) crushing performance on live mollusks. Common mussels (*Mytilus edulis*) are in dark grey, dogwinkles (*Nucella lamellosa*) are in medium grey, and varnish clams (*Nuttalia obscurata*) are in light grey. Boxes represent 50% quantiles, bars represent median values, whiskers represent standard errors, and black dots represent outlying data. Jaw morphologies of each taxon are shown below.

versus 188 N (for *Aetobatus*) as statistically significant. The use of metal models isolated the effect of the morphology of the jaws from any material differences in the jaws and from any effect of the shape and interdigitating pattern of the teeth. In addition to the musculoskeletal differences among these stingrays, we might expect that the tooth interdigitation pattern, long recognized as a taxonomic character (Claeson et al., 2010), has some effect on crushing performance. Regardless, the forces necessary to crush any of the examined live prey (from 22 to 486 N, peak loading) were well within the performance bounds (>500 N) calculated for *Rhinoptera bonasus*, the only myliobatid ray for which bite force has been examined to date (Kolmann et al., 2015). However, evidence by Fisher et al. (2011) has shown that *Rhinoptera* can consume some large oysters requiring in excess of 800–1000 N to

Journal of Experimental Biology (2015) 218, 3941-3949 doi:10.1242/jeb.127340

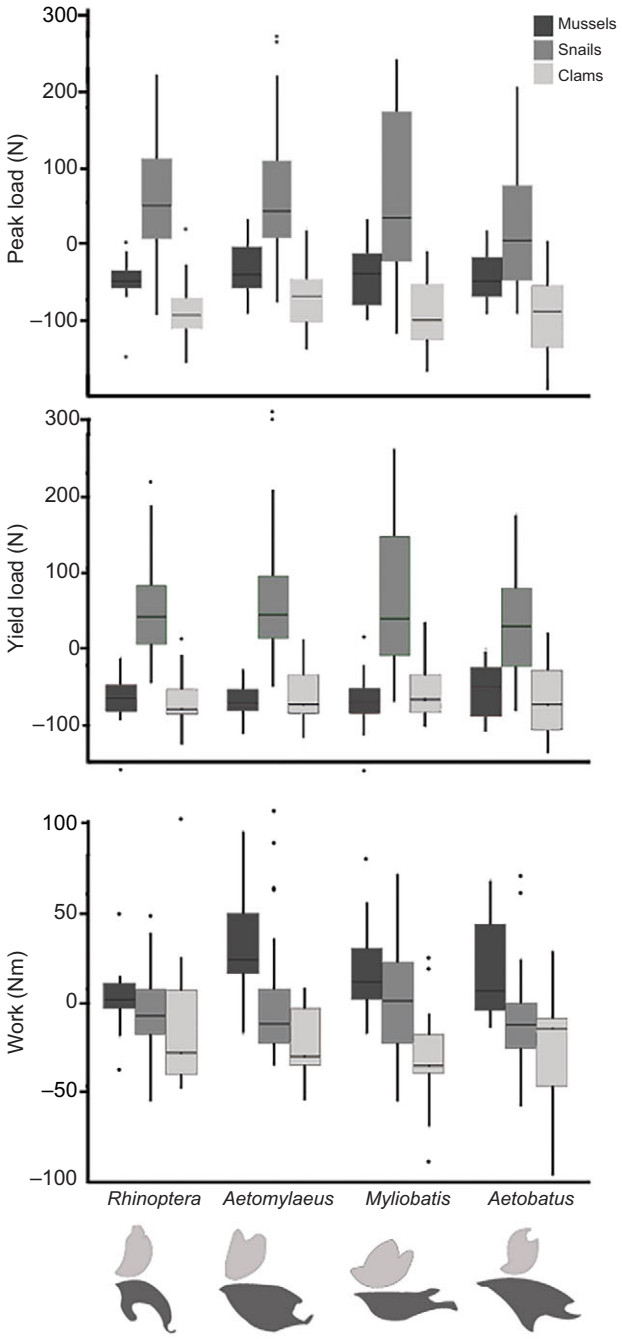

Fig. 5. Box whisker plots showing size-corrected crushing performance on live mollusks. Common mussels (*Mytilus edulis*) are in dark grey, dogwinkles (*Nucella lamellosa*) are in medium grey, and varnish clams (*Nuttalia obscurata*) are in light grey. Performance is size-corrected by taking the residuals of the linear regression of shell height on the respective performance metric (peak and yield loading, work-to-fracture). Boxes represent 50% quantiles, bars represent median values, whiskers represent standard errors, and black dots represent outlying data. Jaw morphologies of each taxon are shown below.

crush. These crushing behaviors on the largest oysters took *Rhinoptera* in excess of 60 min, a duration that seems at odds with the low energy expenditure/high energy gain strategies predicted by optimal foraging theory. Perhaps the curvature of the jaws in these stingrays conveys some performance advantage at prey size extremes that our experimental design could not replicate.

Fig. 6. Evident fracture patterns in *Nucella* shell models. Printed and live gastropods consistently showed crack formation at the base of the spire in almost all trials. Crack propagation continued dorsally along the spire suture, paralleling the shell aperture. This pattern was repeated across shells regardless of shell size.

Artificial prey, either simple (tubes) or complex (3D printed shells), had less individual variation in crushability than live prey, as previously proposed (Crofts and Summers, 2014). Although artificial prey and live snails were found to be significantly different from one another in terms of the magnitude of loading required to fracture their skeleton (2.0–3.0 times greater in printed prey), printed shells approximated the general mechanical behavior of live snails. That is, both live and 3D-printed gastropods showed consistent fracture patterns, with stress fractures occurring at the base of the shell spire and then continuing dorsally along the spire suture. Work-to-fracture was indistinguishable between artificial prey and live *Nucella*, suggesting that this important characteristic of shell material can be mimicked by a powder-based 3D printer. We confirm that replica shells can provide an important proxy for investigations of failure mechanics, clarifying that features other than shell shape (e.g. shell material and structural properties) could contribute to inter-individual variation in failure properties.

Live prey species differed significantly from one another in their ability to absorb energy before fracture (work) and to withstand high forces (loading) before total failure. *Nucella* and *Nuttalia* were stiffer and required higher forces to crush, whereas *Mytilus* required greater energy investment per unit size. This suggests that inherent species-specific differences in shell properties (e.g. shell materials, gross morphologies, and microarchitectures) provide different strategies for avoiding predation that, in turn, perhaps, demand suites of feeding behaviors from predators with diverse diets (e.g. the species examined in this study). In this way, the predator and prey communities are shaping not only each other's ecologies, but also the material and mechanical properties of their skeletal and dental structures. This is underlined by fossil data: prior to the Jurassic, most mollusks were predominantly thin-shelled, non-ornamented, stationary, and epifaunal (Vermeij, 1977), whereas modern molluscan morphology and ecology are thought to have been precipitated by the rise of durophagous predators during the late Mesozoic (75–65 mya).

Our results show little direct relationship between crushing performance and jaw shape in durophagous stingrays, despite observed variation in diet among these taxa. This may indicate that the jaws of durophagous stingrays are an example of 'many-to-one mapping', where multiple and varied morphologies meet the performance requirements for a certain ecological role (e.g. hard prey crushing) (Wainwright et al., 2005). This pattern is common across the vast diversity of vertebrate feeding morphologies in the

context of dietary specialization (Wainwright et al., 2005; Young et al., 2007). Although most previous studies of elasmobranch durophagy have focused primarily on musculoskeletal specializations for eating hard prey (e.g. Kolmann and Huber, 2009; Mara et al., 2010), anecdotal evidence suggests that the diversity of strategies for durophagy in elasmobranchs has only begun to be characterized. For example, the bonnethead shark (*Sphyrna tiburo*) and the horn shark (*Heterodontus francisci*) both purportedly use rapid, repeated jaw contractions to crush prey (Wilga and Motta, 2000; Huber et al., 2005; Mara et al., 2010), a method of cyclical loading to fatigue stiff exoskeletal materials that has also been documented in durophagous crabs (Kosloski and Allmon, 2015). In our study, we only tested the effects of constant rates of compression, but observations of myliobatid prey capture suggest that they may also use cyclical jaw movements in prey crushing (Sasko et al., 2006). Additionally, Mara et al. (2010) suggested that bonnethead sharks may also use low pH stomach activity to supplement their comparatively low bite forces and to further reduce hard-shelled prey to something more easily digestible. Therefore, although high bite forces are clearly paramount for processing hard prey, durophagous elasmobranch taxa may use a suite of not necessarily mechanical methods to reduce prey, suggesting that in elasmobranchs, the concept of 'many-to-one mapping' needs to be expanded to include more than just morphological variation.

Our results underline that durophagous vertebrates are more morphologically variable than previously expected (Crofts and Summers, 2014), even among closely related taxa, highlighting the potential for alternative functional strategies in high-performance systems. The requirement for durophagous taxa to resist high loadings and accumulative fatigue is imperative to the survival of these animals, which tend to have delayed maturity and be generally long-lived (Schluessel et al., 2010; Fisher et al., 2013). As myliobatid jaws appear to represent a 'many-to-one' system in terms of prey crushing performance, further work is required to determine why the jaws exhibit such disparate curvatures across species. Our study focused on shape parameters; however, other yet-to-be-examined features may dictate performance differences among these stingrays, either hard anatomy (skeletal and/or dental), soft anatomy (tendons and/or muscles), or physiology (e.g. gut chemistry). Finally, durophagous systems are frequently highlighted for their mechanical performance or structural strength, but infrequently are both paradigms considered simultaneously, especially in relation to prey structural or material properties. Properties of prey are frequently overlooked in the typical reliance on just one aspect of performance (e.g. bite force). The work and energy required to process prey may relate more intimately to optimal foraging strategies than purely physiological estimates (e.g. maximum bite force), especially when feeding behaviors may be more complex than simply biting with as much force as possible.

Acknowledgements
We dedicate this manuscript to Sonja Fordham, Jeremy Vaudo, Neil 'the Deal' Aschliman, Chris Bedore, Matt Ajemian, Julie Neer, and Dean Grubbs as both proponents and provocateurs in research on durophagous stingrays. We thank Stacy Farina, Nick Gidmark, and Misty Paig-Tran for troubleshooting issues regarding experimental design, software quirks, hardware malfunctions, and theoretical considerations. Jeremy J. Lomax in particular was invaluable when providing assistance for aluminum milling, as well as the Friday Harbor Laboratory maintenance and shop team. Ronald Seidel helped with segmentation of CT scans for this project. Joe Bizzarro, Jeremy Vaudo, Janne Pfeiffenberger, and Gregory Erickson provided immeasurable advice regarding ideas and general discussions of durophagy regarding this manuscript and elsewhere. Cassandra Donnatelli, Matthew Tietbohl, and Anna Conrades helped collect live mollusks and other materials for this project. I (M.A.K.) also thank all my colleagues at Friday Harbor Laboratories for providing an enthusiastic, titillating work environment throughout the duration of my tenure there. Finally, we thank Sigma Xi, Florida State Coastal and Marine Laboratory, and the National Science Foundation for funding that contributed to the gathering of preliminary data for this project idea.

Competing interests
The authors declare no competing or financial interests.

Author contributions
M.A.K., S.B.C. and A.P.S. designed experiments. M.A.K. gathered and analyzed data. N.R.J. and A.P.S. provided financial support for travel and experimentation. M.A.K. and A.P.S. led the writing, and all authors contributed to the final version of the manuscript.

Funding
This work was supported by the National Science Foundation [IOS-1256602 and DBI-1262239 to A.P.S.], a Natural Sciences and Engineering Research Council of Canada Discovery Grant to N.R.L., an HFSP Young Investigators Grant (RGY0067-2013) and DFG-FR 2190/4-1 Gottfried Wilhelm Leibniz-Preis 2010 to M.N.D., and an Ontario Trillium Scholarship to M.A.K.

Supplementary information
Supplementary information available online at
http://jeb.biologists.org/lookup/suppl/doi:10.1242/jeb.127340/-/DC1

References
Ajemian, M. J. and Powers, S. P. (2012). Habitat-specific feeding by cownose rays (*Rhinoptera bonasus*) of the northern Gulf of Mexico. *Environ. Biol. Fish.* **95**, 79-97.
Aschliman, N. C. (2014). Interrelationships of the durophagous stingrays (Batoidea: Myliobatidae). *Environ. Biol. Fish.* **97**, 967-979.
Aschliman, N. C., Nishida, M., Miya, M., Inoue, J. G., Rosana, K. M. and Naylor, G. J. P. (2012). Body plan convergence in the evolution of skates and rays (Chondrichthyes: Batoidea). *Mol. Phylogenet. Evol.* **63**, 28-42.
Bertness, M. D. and Cunningham, C. (1981). Crab shell-crushing predation and gastropod architectural defense. *J. Exp. Mar. Biol. Ecol.* **50**, 213-230.
Capape, C. (1977). Etude du regime alimentaire de la Mourine vachette, *Pteromylaeus bovinus* (Geoffroy Saint-Hilaire, 1817) (Pisces, Myliobatidae) des cotes tunisiennes. *ICES J. Mar. Sci.* **37**, 214-220.
Claeson, K. M., O'Leary, M. A., Roberts, E. M., Sissoko, F., Bouaré, M., Tapanila, L., Goodwin, D. and Gottfried, M. D. (2010). First Mesozoic record of the stingray *Myliobatis wurnoensis* from Mali and a phylogenetic analysis of Myliobatidae incorporating dental characters. *Acta Palaeontol. Pol.* **55**, 655-674.
Collins, A. B., Heupel, M. R., Hueter, R. E. and Motta, P. J. (2007). Hard prey specialists or opportunistic generalists? An examination of the diet of the cownose ray, *Rhinoptera bonasus*. *Mar. Freshw. Res.* **58**, 135-144.
Crofts, S. B. and Summers, A. P. (2014). How to best smash a snail: the effect of tooth shape on crushing load. *J. R. Soc. Interface* **11**, 20131053.
Currey, J. D. (1980). Mechanical properties of mollusk shell. In *The Mechanical Properties of Biological Materials* (ed. J. F. Vincent and J. D. Currey), pp. 75-98. Cambridge, UK: Press Syndicate of the University of Cambridge.
Dean, M. N., Bizzarro, J. J. and Summers, A. P. (2007). The evolution of cranial design, diet, and feeding mechanisms in batoid fishes. *Int. Comp. Biol.* **47**, 70-81.
Fisher, R. A., Call, G. C. and Grubbs, R. D. (2011). Cownose ray (*Rhinoptera bonasus*) predation relative to bivalve ontogeny. *J. Shellfish Res.* **30**, 187-196.
Fisher, R. A., Call, G. C. and Grubbs, R. D. (2013). Age, growth, and reproductive biology of cownose rays in Chesapeake Bay. *Mar. Coast. Fish.* **5**, 224-235.
Gray, A. E., Mulligan, T. J. and Hannah, R. W. (1997). Food habits, occurrence, and population structure of the bat ray, *Myliobatis californica*, in Humboldt Bay, California. *Environ. Biol. Fish.* **49**, 227-238.
Huber, D. R., Eason, T. G., Hueter, R. E. and Motta, P. J. (2005). Analysis of the bite force and mechanical design of the feeding mechanism of the durophagous horn shark *Heterodontus francisci*. *J. Exp. Biol.* **208**, 3553-3571.
Kolmann, M. A. and Huber, D. R. (2009). Scaling of feeding biomechanics in the horn shark *Heterodontus francisci*: Ontogenetic constraints on durophagy. *Zoology* **112**, 351-361.
Kolmann, M. A., Huber, D. R., Dean, M. N. and Grubbs, R. D. (2014). Myological variability in a decoupled skeletal system: batoid cranial anatomy. *J. Morphol.* **275**, 862-881.

Kolmann, M. A., Huber, D. R., Motta, P. J. and Grubbs, R. D. (2015). Feeding biomechanics of the cownose ray, *Rhinoptera bonasus*, over ontogeny. *J. Anat.* **227**, 341-351.
Kosloski, M. E. and Allmon, W. D. (2015). Macroecology and evolution of a crab 'super predator', *Menippe mercenaria* (Menippidae), and its gastropod prey. *Biol. J. Linn. Soc*. **116**, 571-581.
Jardas, I., Santic, M. and Pallaoro, A. (2004). Diet composition of the eagle ray, *Myliobatis aquila* (Chondrichthyes: Myliobatidae), in the eastern Adriatic Sea. *Cybium* **28**, 372-374.
Mara, K. R., Motta, P. J. and Huber, D. R. (2010). Bite force and performance in the durophagous bonnethead shark, *Sphyrna tiburo*. *J. Exp. Zool. A* **313**, 95-105.
Mulvany, S. and Motta, P. J. (2014). Prey capture kinematics in batoids using different prey types: Investigating the role of the cephalic lobes. *J. Exp. Zool. A Ecol. Genet. Physiol.* **321**, 515-530.
Pfaller, J. B., Gignac, P. M. and Erickson, G. M. (2011). Ontogenetic changes in jaw-muscle architecture facilitate durophagy in the turtle *Sternotherus minor*. *J. Exp. Biol.* **214**, 1655-1667.
Sasko, D. E., Dean, M. N., Motta, P. J. and Hueter, R. E. (2006). Prey capture behavior and kinematics of the Atlantic cownose ray, *Rhinoptera bonasus*. *J. Zool.* **109**, 171-181.
Schluessel, V., Bennett, M. B. and Collin, S. P. (2010). Diet and reproduction in the white-spotted eagle ray *Aetobatus narinari* from Queensland, Australia and the Penghu Islands, Taiwan. *Mar. Freshw. Res.* **61**, 1278-1289.
Summers, A. P. (2000). Stiffening the stingray skeleton – an investigation of durophagy in myliobatid stingrays (Chondrichthyes, Batoidea, Myliobatidae). *J. Morphol.* **243**, 113-126.
Szczepanski, J. A. and Bengston, D. A. (2014). Quantitative food habits of the bullnose ray, *Myliobatis freminvillii*, in Delaware Bay. *Environ. Biol. Fish.* **97**, 981-997.
Vermeij, G. J. (1977). The Mesozoic marine revolution: evidence from snails, predators and grazers. *Paleobiology* **3**, 245-258.
Wainwright, P. C., Alfaro, M. E., Bolnick, D. I. and Hulsey, C. D. (2005). Many-to-one mapping of form to function: a general principle in organismal design?. *Integr. Comp. Biol.* **45**, 256-262.
Whitenack, L. B. and Herbert, G. S. (2015). Did shell-crushing crabs trigger an escalatory arms race in the aftermath of a Late Neogene regional mass extinction event? An experimental test. *Palaeogeogr. Palaeoclimatol. Palaeoecol.* **417**, 57-65.
Wilga, C. D. and Motta, P. J. (2000). Durophagy in sharks: feeding mechanics of the hammerhead *Sphyrna tiburo*. *J. Exp. Biol.* **203**, 2781-2796.
Yamaguchi, A., Kawahara, I. and Ito, S. (2005). Occurrence, growth and food of longheaded eagle ray, *Aetobatus flagellum*, in Ariake Sound, Kyushu, Japan. *Environ. Biol. Fish.* **74**, 229-238.
Young, R. L., Haselkorn, T. S. and Badyaev, A. V. (2007). Functional equivalence of morphologies enables morphological and ecological diversity. *Evolution* **61**, 2480-2492.

Table S1 & S2

Click here to Download Table S1 & S2